Flexible 2D Laser Cutting of Ultra-Thin Glass Using an Ultrashort Pulsed Laser Robotic System

Daniel Franz[*1], Yongting Yang[1], Cemal Esen[2] and Ralf Hellmann[1]

[1]*Applied Laser and Photonics Group,*
University of Applied Sciences Aschaffenburg,
Würzburger Str. 45, 63743 Aschaffenburg, Germany
[2]*Applied Laser Technologies,*
Ruhr University Bochum,
Universitätsstraße 150, 44801 Bochum, Germany
[*]*Corresponding author's e-mail: Daniel.Franz@th-ab.de*

We report for the first time on the flexible and large-area 2D laser cutting of ultra-thin glass using an ultrashort pulsed laser robot (USPLR) system emitting at a wavelength of 1030 nm. To optimize the cutting quality of 100 µm thick AF 32 eco ultra-thin glass substrate, experiments were performed with different laser pulse durations, laser pulse energies, laser pulse repetition rates and robot speeds. For the evaluation of the cutting quality, crack formation and induced stresses near the cutting edge were analyzed using imaging polarimetry and digital microscopy. At robot speeds of up to 40 mm/s, crack formation occurs at laser pulse durations greater than 1 ps. Using a laser pulse duration of 1 ps, laser pulse energies of up to 140 µJ and a laser pulse repetition rate of 200 kHz, complete cuts are produced in a wide processing window at robot speeds of 15 mm/s to 65 mm/s without crack formation. In addition, when using a laser pulse repetition rate of 400 kHz and a laser pulse energy of 80 µJ, the processing window is extremely enlarged due to heat accumulation effects. However, at the high robot speeds of up to 80 mm/s, unevenness and notching of the cutting edges are observed as a result of vibrations of the USPLR system during laser cutting, limiting the potential processing speed. An ultra-thin glass component is produced with sharp and rounded cutting edges, demonstrating the high potential of the USPLR system for the flexible and large area 2D laser cutting applications in various industrial sectors.
DOI: 10.2961/jlmn.2026.01.2004
Keywords: ultrashort pulsed laser, robot, laser cutting, ultra-thin glass, AF 32 eco, polarimetry.

1. Introduction

The growing demand for high-precision and damage-free processing of glass materials in both science and technology has led to the increased use of ultrashort pulsed (USP) lasers for micromachining in recent years. The ablation mechanism of glass is enabled by non-linear absorption mechanisms as a result of the very high pulse peak intensities [1; 2]. With laser pulse durations in the picosecond and femtosecond range, the thermal load during USP laser processing with small focal spot sizes is negligible due to the so-called cold ablation process [3; 4].

The gentle and favourable laser-material interaction is particularly exploited in laser cutting of ultra-thin glass (UTG) substrates with thicknesses of ≤ 100 µm. Such thin glasses are required for the manufacturing of flexible and high-power electronics [5-7], advanced display applications [8; 9], flexible energy technology [10; 11] and microfluidics [12; 13]. Compared to conventional mechanical dicing, laser-based cutting offers a higher cut quality through reduced chipping and micro-crack formation. Furthermore, although conventional methods are simple and inexpensive, the induced residual stresses and inadequate cutting edge quality require post-processing such as grinding, polishing and heat treatment to meet industrial requirements, increasing cutting costs and time [14-16].

Using a galvanometer scanner combined with a telecentric f-theta lens and a laser pulse duration of 6 ps,

Wlodarczyk et al. [16] report on laser cutting of various UTG substrates with different thicknesses and laser wavelengths. For laser cutting of a 100 µm thick AF 32 eco glass substrate, a high cutting quality is achieved using multiple scanning at an effective cutting speed of up to 100 mm/s and a wavelength of 515 nm. Small heat-affected zones of < 25 µm are also obtained, as well as low debris on the glass surface. Markauskas et al. [4] perform multi-scan laser cutting of various thicknesses of borosilicate glass down to 110 µm in ambient air and water using a galvanometer scanner and an f-theta lens. The experimental studies show that femtosecond laser cutting quality of UTG substrates is comparable in both environmental conditions. Chipping and cracking with mean and maximum defect widths of 6.1 µm and 15 µm are observed, respectively.

Femtosecond UTG laser cutting, considering the effective cutting speed and the edge strength using a focusing lens and a translation stage, is reported by Shin et al. [17] using a Ti:Sapphire laser. Experimental studies show a strong dependence of edge strength on the polarization of the laser radiation, with perpendicular polarization to the cutting path producing faster and cleaner cuts as compared to parallel polarization. High mechanical strength is achieved when using a laser overlap ratio of 0.99 and a laser fluence of 19 J/cm², which is attributed to the smooth, defect free cutting surface. In addition, the authors also introduce a bottom-up cutting
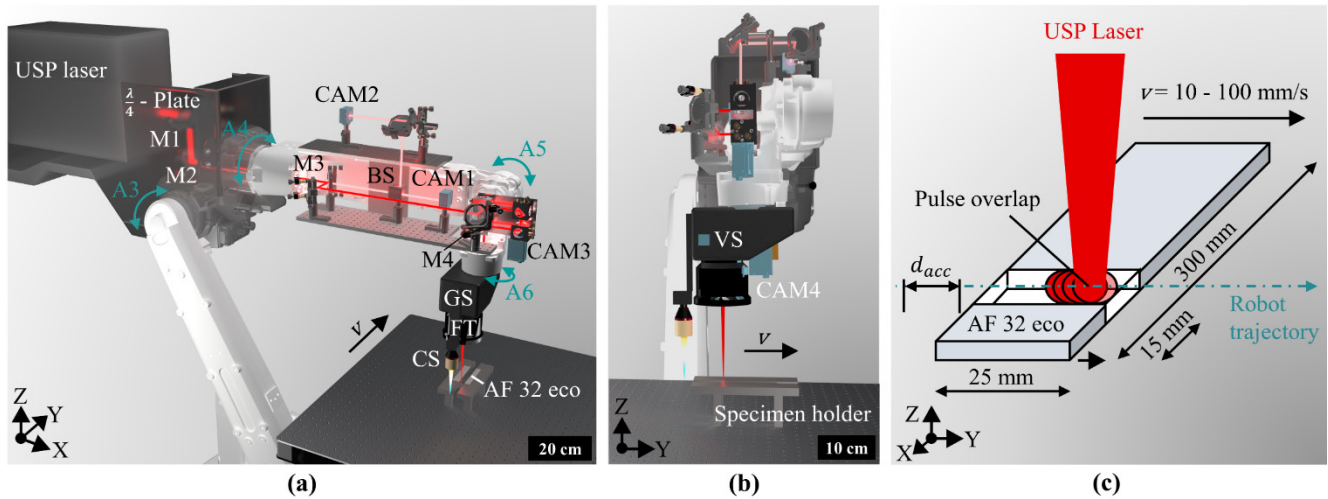
Fig. 1 Overview of the USPLR system used for laser cutting experiments of AF 32 eco thin glass with a USP laser mounted on robot axis A3 on a 6-axis articulated industrial robot. The laser beam is guided mirror-based along robot axes A3 to A6, where a 2D galvanometer scanner (GS) and a telecentric f-theta lens (FT) are used to deflect and focus the laser beam within the focal plane, respectively. A confocal distance sensor (CS) is applied for laser focus monitoring. A two-stage beam position stabilization concept consisting of a total of 4x piezoelectric mirror elements (M) and 4x CMOS camera sensors (CAM) is implemented to compensate dynamic beam position deviations. A vibration sensor (VS) is mounted on robot axis A6 to monitor vibrations during laser cutting experiments. (a) Side view. (b) Front view (c) Schematic of laser cutting.

method for optimizing the edge strength by eliminating bottom and backside ablation [14]. Compared to a conventional femtosecond laser cutting strategy, the front and back edge strength of the glass is increased by up to 65 % to a maximum of ~380 MPa.

In addition to conventional through-glass laser cutting using galvanometer scanners, focusing lenses and translation stages, indirect cutting methods such as laser scribing and laser cleaving are the most commonly used methods for dicing mainly thicker glass substrates [19-25]. Only a few studies have dealt with laser cleaving of UTG substrates [18, 26; 27]. In this process, picosecond and femtosecond laser pulses are used to locally ablate or modify the glass on the top or back surface or within the material. The glass is then separated by targeted mechanical or thermal stress [18; 22]. Recently, the use of Bessel beams in combination with USP lasers for internal scribing of thick glass substrates has been introduced, where the cutting edge is subsequently produced by a mechanical breaking step. Due to non-linear absorption processes, thread-like damage along a filamentary propagation through the entire glass thickness is achieved by non-linear absorption due to the extremely high energy density [18; 22; 28-31].

As an alternative to these introduced USP laser-based glass cutting techniques, we report for the first time on a comprehensive study for flexible and large-area ultra-thin glass cutting using an USP laser robotic (USPLR) system. To evaluate the cutting quality after laser processing with different laser pulse durations, laser pulse energies, laser pulse repetition rates and robot axis speeds, we analyze the formation of cracks and the residual stresses near the cutting edge using imaging polarimetry.

2. Experimental
2.1 Laser Robot System

A USP laser (Light Conversion, CB3-40W) with a wavelength of 1030 nm, integrated on robot axis A3 of a 6-axis articulated industrial robot (ABB, IRB 2600ID-8/2.00) is used for flexible and large-area 2D laser cutting of UTG substrates, see Fig. 1 (a, b). The laser beam is guided along robot axis A3 to robot axis A6 by mirrors. On robot axis A6, a combination of a 2D galvanometer scanner (GS) (Newson, RTAX-A15) and a telecentric f-theta lens (FT) with a focal length of 160 mm (Jenoptik, JENar Silverline F-Theta) is used to deflect and focus the circular polarized laser beam. The combination yields a laser focus diameter of approximately 64 µm and a Rayleigh length of 2,582 µm. Latter is an important characteristic in laser micromachining as it defines the distance from the laser focal diameter at which the waist of the beam expands by a factor of $\sqrt{2}$, resulting in halved laser intensity [32]. To achieve high-quality and complete cuts, precise focusing with the USPLR system is mandatory to ensure a constant energy distribution along the cutting trajectory, in turn, mainly determined by the laser focus diameter and the pulse overlap. A confocal distance sensor (CS) (Keyence, CL-L070) is used to monitor the laser focus level on the glass surface. An innovative two-stage concept for beam position stabilization on robot axes A4 and A5 is applied, which is based on the detection of the laser beam centers by CMOS image sensors (CAM) (The Imaging Source, 2x DMK 37AUX250, 2x DMK 38UX541) and their control by piezoelectric driven mirrors (M) (Thorlabs, 4x
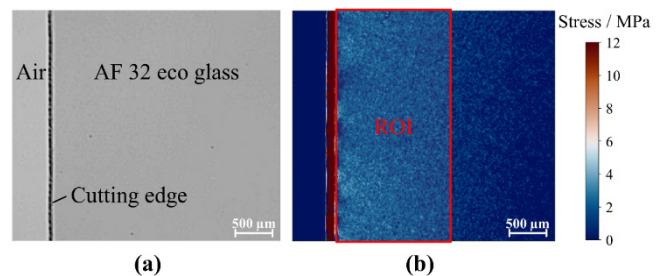

Fig. 2 Determination of thermally induced stresses after laser cutting using imaging polarimetry. (a) Optical image. (b) Analysis of residual stresses.

PIAK10). The authors provide in Ref. [33-34] detailed information on the operating principle of the beam position control.

2.2 Material and Methods

For laser cutting, 300 mm × 300 × mm × 0.1 mm (length × width × thickness) AF 32 eco UTG sheets (Schott AG, Germany) were cut into approximately 25 mm × 300 mm long strips using the USPLR system, cf. Fig. 1 (c). These strips were in turn cut into small glass samples of approximately 25 mm × 15 mm using different laser pulse durations, laser pulse repetition rates, laser pulse energies and robot axis speeds. Laser cutting was performed only in the y-direction of the robot system. In order to evaluate the cutting quality in dependence of different laser parameters, thermally induced stresses and crack formation near to the cutting edge were investigated after laser processing using imaging polarimetry (ilis, StrainScope Flex) and digital microscopy (Leica, DMV6 a). An overview of the constant and varied laser parameters used for the laser cutting experiments is given in Table 1. The optical retardation is determined within a field of view of 800 × 600 pixel with a pixel size of 10.25 µm in square. The residual stress in the glass after laser cutting is then calculated as follows

$$\sigma = \frac{\delta}{t \cdot C}, \qquad (1)$$

where δ is the optical retardation, t the thickness of the glass and C the stress optical coefficient. Please note that for a number of experiments of $N = 3$, only complete laser cuts without the formation of cracks were analyzed. In the center of the glass sample, residual stresses near to the cutting edge is determined within a region of interest (ROI) of 350 × 150 px, cf. Fig. 2 (b). To compare the laser cutting quality using different laser parameters, the sum of the total induced residual stresses within the ROI is used.
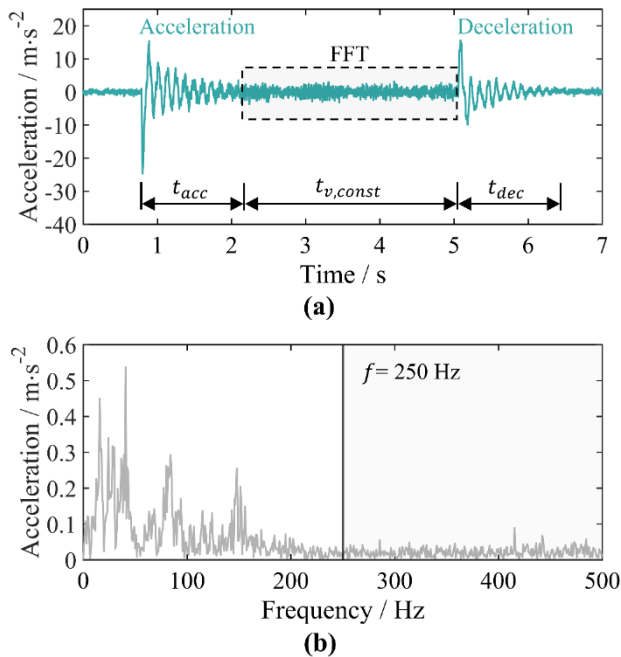
Fig. 3 Exemplary acceleration signal in y-direction during a robot movement over a total distance of 400 mm at a robot speed of 70 mm/s. (a) Time domain. (b) Frequency domain.
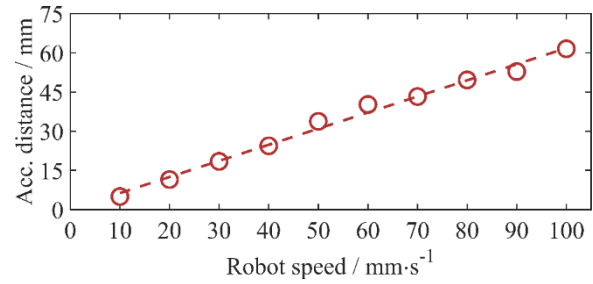
Fig. 4 Required acceleration distance in dependence of the robot speed to ensure constant laser pulse overlap.

Uneven cut edges are observed during laser cutting experiments at different laser robot speeds. Therefore, a triaxial vibration sensor (VS) (PCB Piezotronics, model PCB-356A15) is mounted on robot axis A6 to analyze the vibrations along a movement of the USPLR system over a total distance of $d_{total} = 400$ mm, cf. Fig. 2 (b). As an example, the acceleration signal in the y-direction at a robot speed of 70 mm/s as a function of time is shown in Fig. 3. In order to evaluate the vibrations in the x-, y- and z-directions during the robot movement in the frequency domain, the one-dimensional Fast Fourier Transformation (1D FFT) is used for the signal domain with a constant robot axis speed, which in turn is the case when no acceleration is observed, cf. Fig. 3 (a). Please note that only frequencies up to $f = 250$ Hz are considered in the FFT evaluation, as at higher frequencies only noising is observed. In addition, to ensure a constant laser pulse overlap due to a constant robot speed and thus to guarantee a constant processing quality, the required acceleration distance d_{acc} was calculated before UTG cutting experiments as follows

$$d_{acc,dec} = \frac{(d_{total} - v \cdot t_{v,const})}{2}, \qquad (2)$$

where v is the robot axes speed, d_{total} is the total distance of robot movement and $t_{v,const}$ is the time interval at constant robot speed. Thereby, to simplify matters, it is assumed that the distance required for acceleration is the same as compared to that for the deceleration process.

Table 1 Overview of the variable and constant laser parameters used for AF 32 eco UTG cutting experiments with the USPLR system.

Variable parameter	
Laser pulse duration / ps	0.23 - 8
Laser pulse repetition rate / kHz	200, 400
Laser pulse energy / µJ	80 - 140
Laser fluence / J·cm^{-2}	2.49 - 4.35
Robot axes speed / mm·s^{-1}	10 - 100
Laser pulse overlap / %	99.23 - 99.96

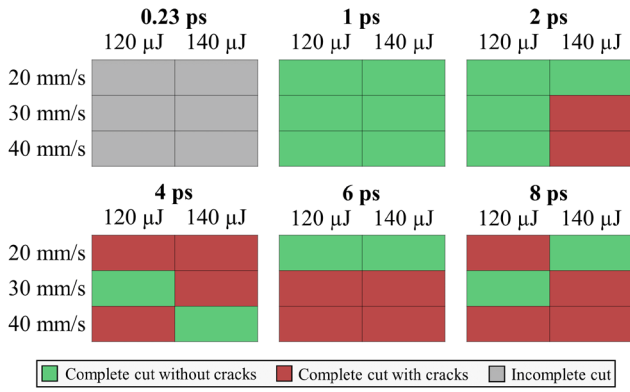| Constant parameter	
Wavelength / nm	1,030
Beam quality M^2	< 1.2
Laser focus diameter / µm	64
Rayleigh length / µm	2,582

Fig. 5 Categorization maps of the laser cutting quality using different laser pulse durations, laser pulse energies and robot speeds.

The results of the obtained acceleration distances in dependence of the robot axes speed of the USPLR system up to 100 mm/s are shown in Fig. 4, revealing a linear relationship between the acceleration distance and the robot speed with $d_{acc} = 0.62 \cdot v$. To ensure a constant pulse overlap during the cutting, the acceleration distance is taken into account by offsetting the starting point of the laser cutting with the USPLR system in relation to the glass strips, cf. Fig. 1 (c).

3. Results and Discussion
3.1 Laser Pulse Duration

To determine the influence of different laser pulse durations on UTG cutting quality, glass samples were cut using laser pulse energies of 120 µJ and 140 µJ, a robot speed of 20 mm/s - 40 mm/s and a laser pulse repetition rate of 200 kHz. The categorization maps in Fig. 5 differentiate the laser cutting quality in terms of complete and incomplete cuts and the formation of cracks in dependence of the laser pulse duration of 0.23 ps - 8 ps.

For all laser parameters and robot speeds, UTG substrates were not cut through sufficiently using a femtosecond laser pulse duration. In addition, small processing windows are observed for a laser pulse duration greater than 2 ps. Only when using a laser pulse duration of 1 ps, glass samples were completely cut without crack formation within the entire investigated laser parameter range. As an example, Fig. 6 exemplifies the laser cutting edge and the induced stress

after laser processing with different laser pulse durations for a laser pulse energy of 140 µJ and a robot speed of 30 mm/s using optical images and imaging polarimetry. The influence of the laser pulse duration is clearly visible, where for laser pulse durations in a range of 2 ps - 8 ps significantly larger laser induced stress and crack formation is observed near the cutting edge. We attribute this dependence to an increased heat accumulation, which is more pronounced in single-path laser cutting due to the high laser pulse overlap of more than 99 % used (cf. Table 1) and to an extended heat diffusion for longer pulses (here a factor of 7 - 8 using available thermal properties of the material supplier for a laser pulse duration increase from 0.23 ps to 8 ps), both in turn leading to a sensitive alteration of the contributions of sublimation and fusion cutting [35-38]. If a critical stress value is locally exceeded during laser cutting, cracks will form to relieve the thermally induced stresses [16; 39; 40]. In addition, stronger stress waves are generated for picosecond laser pulses, which also influence the formation of cracks [36]. In order to further optimize the cutting quality of AF 32 eco UTG by adjusting the laser parameters without the formation of cracks, subsequent experiments were carried out with a laser pulse duration of 1 ps.

3.2 Laser Pulse Energy, Robot Speed and Laser Pulse Repetition Rate

The evaluation of the integrated laser-induced stresses in the AF 32 eco substrate after laser cutting using laser pulse energies of 80 µJ - 140 µJ, laser pulse repetition rates of 200 kHz and 400 kHz, robot speeds of 15 mm/s - 80 mm/s and a laser pulse duration of 1 ps is summarized in Fig. 7. Please note that the UTG strips were analyzed for residual stresses prior to laser cutting experiments in order to provide a stress-free specimen and allow correct analysis of the laser induced stress. It should also be noted that only crack-free glass samples and complete cuts were analyzed for stress after laser cutting using imaging polarimetry.

Considering the averaged stress integrals and the processing window in dependence of the laser pulse energy in the range of 80 µJ - 140 µJ at a laser pulse repetition rate of 200 kHz, it is noticeable that a high laser pulse overlap of greater than 99 % is required to cut through the UTG material with a single pass of the USPLR system. The processing
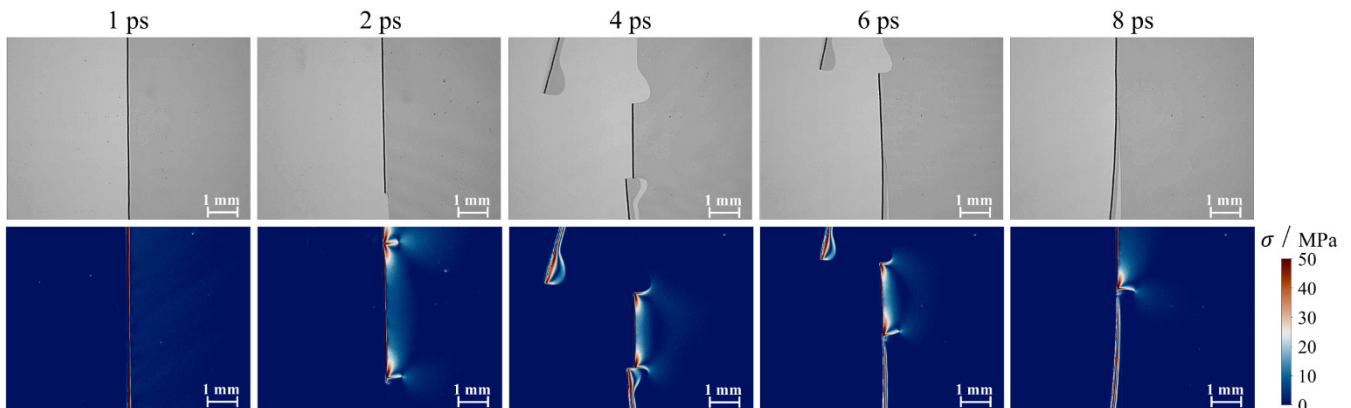

Fig. 6 Evaluation of the crack formation and residual stresses in AF 32 eco UTG after laser cutting with a laser pulse energy of 140 µJ, a laser pulse repetition rate of 200 kHz and a robot speed of 30 mm/s in dependence of different laser pulse durations using optical images (top) and imaging polarimetry (bottom).
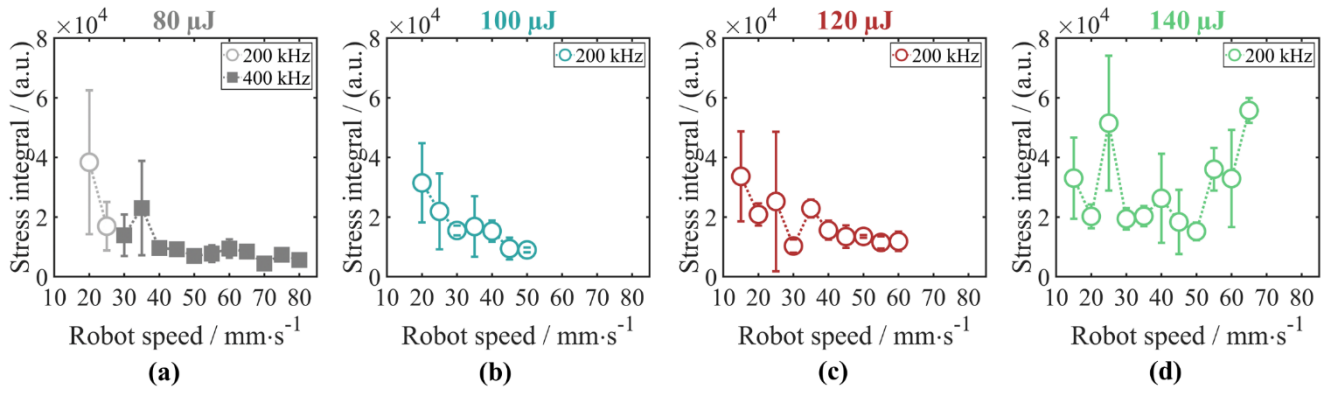
Fig. 7 Evaluation of the integral of residual stresses after laser cutting of UTG in dependence of the laser pulse energy, robot speed and laser pulse repetition rate. Please note that each stress integral represents the average of 3 measurements and its standard deviation. (a) 80 µJ. (b) 100 µJ. (c) 120 µJ. (d) 140 µJ.

window increases steadily with the applied laser pulse energy, with the largest processing window being achieved using a laser pulse energy of 140 µJ at robot speeds of 15 mm/s to 65 mm/s. In addition, it is clearly visible that for higher laser robot speeds, the laser-induced stress and its deviations are significantly reduced for laser pulse energies of 80 µJ - 120 µJ. A minimum stress integral of 8,985 ± 809 on average is reached for a laser pulse energy of 120 µJ at a robot speed of 50 mm/s, cf. Fig. 7 (b). However, this is not the case for the highest laser pulse energy, where significantly higher stress integrals with a maximum of 55,734 ± 4,188 are observed at a robot speed of 65 mm/s. We assume that the accumulated energy input along the cutting edge by using a high laser fluence of 4.35 J/cm^2 combined with the high laser pulse overlaps of more than 99 % cause a significant increase in stress generation during laser cutting.

Besides the adaption of the laser pulse energy, another possibility for minimizing laser-induced stress and enlarging the processing window is the use of a higher laser pulse repetition rate of 400 kHz, as shown in Fig. 7 (a). Please note that the influence of the laser pulse repetition rate could only be investigated at the lowest laser pulse energy of 80 µJ due to the limited power availability of the used USP laser. Complete cuts are observed at robot speeds in a range of 30 mm/s - 80 mm/s for using a laser pulse repetition rate of 400 kHz. Thus, the processing window is extremely enlarged as compared to the use of a laser pulse repetition rate of 200 kHz. In addition, averaged stress integrals are reduced to a minimum of 4,428 ± 1,622 at a robot speed of 70 mm/s. We attribute the significantly enlarged processing window at a higher laser pulse repetition rate of 400 kHz to an increasing heat accumulation along the cutting path, which occurs when the time interval between successive laser pulses is insufficient to remove the residual heat by the heat conduction into the surrounding glass material [16; 39; 41].
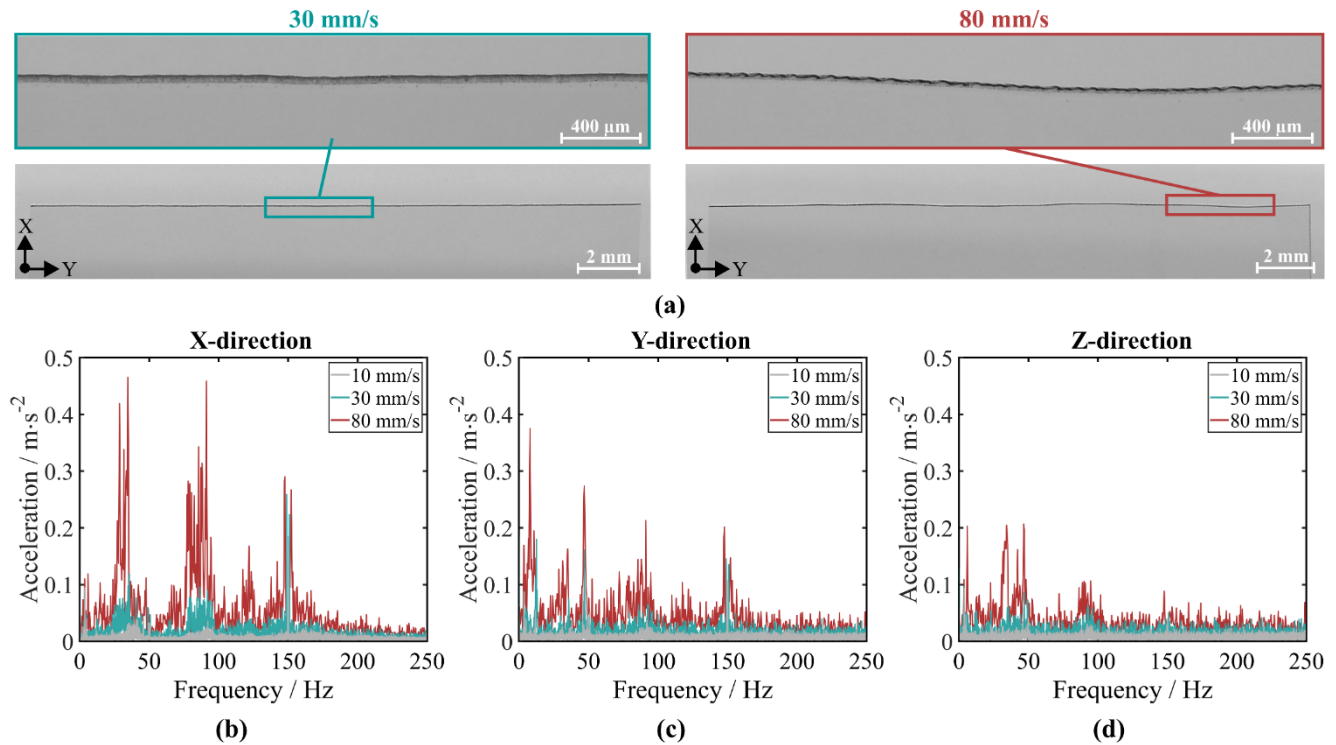

Fig. 8 Evaluation of the three-dimensional vibration frequency during laser cutting experiments in dependence of the robot speed using an acceleration sensor and digital microscopy. (a) Straightness of the cutting edge. (b) X-direction. (c) Y-direction. (d) Z-direction.
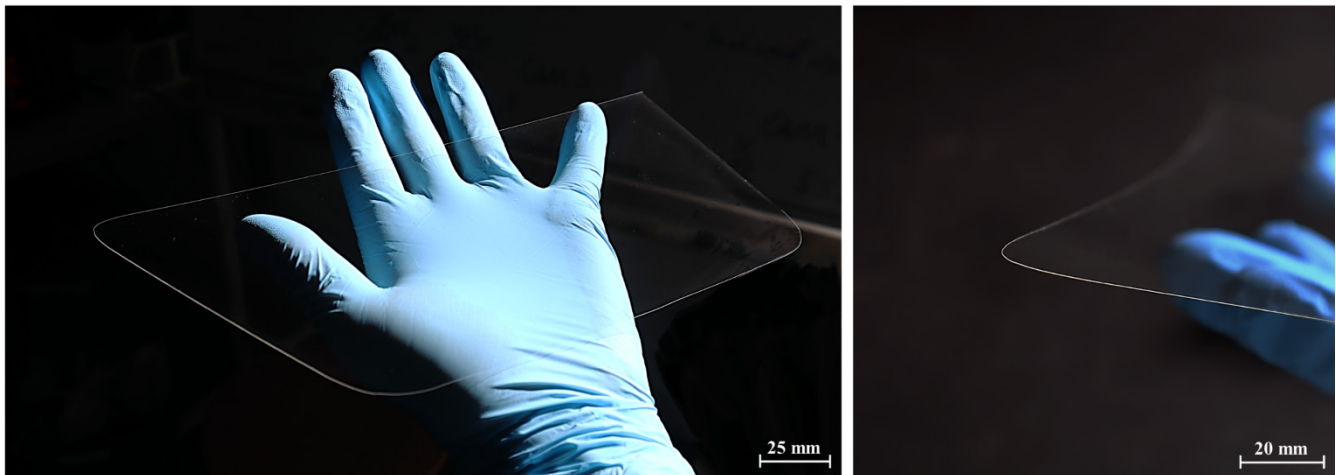
Fig. 9 Demonstration of flexible and large-area 2D laser cutting of AF 32 eco UTG using the USPLR system for an exemplary geometry.

Please note that the introduced single mode cutting method with the USPLR system is also suitable for cutting other UTG materials (Borosilicate UTG D263), as recently reported by the authors in Ref. [42], and is also transferable to further materials such as metal foils and printed circuit board substrates. Details of such applications will be published elsewhere.

3.3 Vibrations of USPLR System

Uneven cut edges are observed during cutting of UTG substrates at various robot speeds of up to 80 mm/s. Examples of optical images of the varying straightness of the AF32 eco glass cut edge at robot speeds of 30 mm/s and 80 mm/s are shown in Fig. 8 (a). It is clearly visible that a straight cutting edge is fabricated at a robot speed of 30 mm/s, whereas at a higher robot speed of 80 mm/s an uneven cut edge is obtained. In addition, the optical image in Fig. 8, top right, shows notches along the cutting edge at a robot speed of 80 mm/s. To determine the cause of the unevenness and notches along the cutting edge, a triaxial vibration sensor was mounted on robot axis A6 and used to analyze the vibrations during the movement in y-direction at different linear robot speeds.

The evaluation of the three-dimensional vibrations in the frequency domain using 1D FFT analysis during the movement of the USPLR system is shown in Fig. 8 (b-d) for different robot speeds in the range of 10 mm/s to 80 mm/s for frequencies up to 250 Hz. The comparison of the measured vibration signals in dependence of their direction shows that the highest and lowest vibrations are obtained in the x- and z-directions, respectively. Using a robot speed of 80 mm/s, maximum vibrations of 0.21 m/s^2 and 0.47 m/s^2 are observed at frequencies of 46.6 Hz and 34.7 Hz in the x-direction and z-direction, respectively.

The vibrations in the x-direction perpendicular to the cutting direction are shown in Fig. 8 (b) for robot speeds of up to 80 mm/s. It is clearly visible that the vibrations are dependent of the robot speed and are mainly localized in three different frequency domains with different magnitudes: (1) 24 Hz - 35 Hz, (2) 75 Hz - 95 Hz and (3) 147 Hz - 153 Hz. Since the vibrations in the third frequency domain are of a similar order of magnitude for different robot speeds and independent of the vibration direction, cf. Fig. 8 (b-d),

we assume that those are inherent to the USPLR system. These vibrations can in turn be attributed to the different centers of mass at different robot axis positions due to the weight of the integrated USP Laser on robot axis A3 and opto-mechanical components, such as brackets, mirrors, the 2D galvanometer scanner and the f-theta lens [43]. Therefore, we attribute the observed uneven cutting edge to the first and second frequency domain, where vibrations significantly increase with higher robot speeds of 30 mm/s and 80 mm/s compared to 10 mm/s. The maximum straightness deviation of the cutting edge at the a robot speed of 30 mm/s and 80 mm/s is 12 μm and 32.8 μm, respectively, which is in the range of approximately half the laser focus diameter, cf. Table 1. Thus, we assume that vibrations in the z-direction are in a range of only a few tens of microns, since the vibrations in x-direction are significantly more pronounced, cf. Fig. 8 (b, d). Comparing the observed maximum straightness deviation to the Rayleigh length of 2,582 μm, cf. Table 1, we conclude that the influence of the fluctuating laser focusing with the USPLR system has a negligible impact on the laser cutting quality.

The vibrations in the y-direction parallel to the cutting direction are depicted in Fig. 8 (c). In addition to the aforementioned inherent frequency domain of the USPLR system in the range of 147 Hz - 153 Hz, others are identified in a range of 2 Hz - 18 Hz, 42 Hz - 52 Hz and 80 Hz - 98 Hz. We attribute the observed notches along the cutting edge for a robot speed of 80 mm/s to a combination of the increasing vibrations in both the x-direction and y-direction, cf. Fig. 8 (a) top right. In contrast, for a lower robot speed of 30 mm/s, a nearly straight cutting edge without visible notches is obtained due to the decreasing vibrations parallel and perpendicular to the direction of robot movement.

3.4 Flexible and Large-Area 2D Laser Cutting of UTG

To demonstrate the flexible and large-area 2D laser cutting of AF 32 eco UTG substrates, an exemplarily chosen geometry is laser-cut using the USPLR system with a laser pulse duration of 1 ps, a laser pulse repetition rate of 200 kHz and 400 kHz and a laser pulse energy of 120 μJ and 80 μJ, respectively. Images of the fabricated glass component with sharp and rounded edges and a size of approximately 235 mm x 120 mm is shown in Fig. 9. Apparently,

the USPLR system is capable to produce both sharp and rounded edges with a high precision and cutting quality. Thus, the innovative laser robotic system is suitable to perform flexible and large-area laser UTG cutting applications required in different industrial sectors, e.g. for advanced displays in the futures vehicle interiors or flexible thin film modules for photovoltaic systems.

4. Conclusion

We have reported on the flexible and large-area 2D laser cutting of AF 32 eco ultra-thin glass using an ultrashort pulsed laser robot with an infrared wavelength. The laser cutting quality in terms of laser-induced stress and crack formation is optimized by using different laser pulse durations, laser pulse energies, laser pulse repetition rates and robot speeds. Using a laser pulse duration of 2 ps - 8 ps, and a laser pulse repetition rate of 200 kHz, crack formation occurs for robot speeds of up to 40 mm/s. The processing window for the use of a laser pulse duration of 1 ps is increased by using a higher laser pulse energy of up to 140 µJ with robot speeds in a range of 15 mm/s - 65 mm/s. For a laser pulse energy of 80 µJ, the processing window is significantly enlarged by applying a higher laser pulse repetition rate of 400 kHz, which is attributed to heat accumulation effects. Though increasing vibrations of the USPLR system at higher robot speeds occur, qualitative large area glass cutting can be achieved at robot speeds of up to 80 mm/s with virtually straight cut lines and clear edges without sheared edge defects such as cracks.

References

[1] X. Liu, D. Du, and G. Mourou: IEEE J. Quantum Elect., 33, (1997) 10.
[2] E. G. Gamaly, A. V. Rode, B. Luther-Davies, and V. T. J. Tikhonchuk: J. Plasma Phys., 9, (2002) 3.
[3] N. A. Inogamov, Y. V. Petrov, V. A. Khokhlov, and V. V. Zhakhovskii: Hig Temp., 58, (2020).
[4] E. Markauskas, L. Zubauskas, G. Račiukaitis, G., and P. Gečys: Micromachines, 14, (2023) 1.
[5] S. Sivapurapu, R. Chen, M. ur Rehman, K. Kanno, T. Kakutani, M. Letz, F. Liu, S. K. Sitaraman, and M. Swaminathan: Proc. IEEE, Vol. 71, (2021).
[6] Z. Wu, J. Min, M. Kim, M. R. Pulugurtha, V. Sundaram, and R. R. Tummala: Proc. IEEE, Vol. 66, (2016).
[7] Y. Lai, K. Pan, and S. Park: Microelectron. Reliab., 161, (2024) 115477.
[8] M. H. Ha, J. K. Choi, B. M. Park, and K. Y. Han: J. Mech. Sci., 35, (2021).
[9] S. M. Garner, K. W. Wu, Y. C. Liao, J. W. Shiu, Y. S. Tsai, K. T. Chen, Y. C. Lai, C. C. Lai, Y. Z. Lee, J. C. Lin, X. Li, and P. Cimo: J. Disp. Technol., 9, (2013) 8.
[10] N. Li, Z. Chen, W. Ren, F. Li, and H. M. Cheng: Proc. Natl. Acad. Sci. USA, 109, (2012) 43.
[11] M. Bedjaoui, J. Amiran, and J. Brun: Proc. IEEE, Vol. 69, (2019).
[12] Y. Yalikun, Y. Hosokawa, T. Iino, and Y. Tanaka: Lab Chip, 16, (2016) 13.
[13] Y. Yalikun, and Y. Tanaka: Sens. Actuators A: Phys., 263, (2017).
[14] H. Shin, J. Noh, and D. Kim: Opt. Laser Technol., 138, (2021).
[15] S. Nisar, L. Li, and M. A. Sheikh: J. Laser Appl., 25, (2013) 4.
[16] K. L. Wlodarczyk, A. Brunton, P. Rumsby, and D. P. Hand: Opt. Laser Technol., 78, (2016).
[17] H. Shin, and D. Kim: Opt. Laser Technol., 102, (2018).
[18] H. Shin, and D. Kim: Opt. Laser Technol., 129, (2020).
[19] Y. Luo, Y. Xie, Z. Zhang, Z. Li, and Y. Huang: Opt. Commun., 555, (2024).
[20] J. Shin: Opt. Laser Technol., 111, (2019).
[21] W. Jung, H. Kim, A. Voronov, S. Park, J. Ryu, S. H. Jeong, and C. L. Roh: J. Inf. Disp., 30, (2022) 5.
[22] C. Ungaro, and A. Liu: Opt. Laser Technol., 144, (2021).
[23] F. Werr, U. Eppelt, L. Müllers, and D. D. Ligny: Front. Phys., 10, (2022).
[24] D. Flamm, M. Kaiser, M. Feil, M. Kahmann, M. Lang, J. Kleiner, and T. Hesse: J. Laser Appl., 34, (2022) 1.
[25] K. Liao, W. Wang, X. Mei, and B. Liu: Ceram. Int., 48, (2022) 7.
[26] H. C. Cheng, K. H. Li, C. Y. Shih, and W. H. Chen: IEEE Trans. Compon. Packag. Manuf. Technol., 8, (2018), 12.
[27] A. Collins, D. Rostohar, C. Prieto, and Y. K. Chan: Opt. Lasers Eng., 60, (2014).
[28] K. Bergner, M. Müller, R. Klas, J. Limpert, S. Nolte, and A. Tünnermann: Appl. Opt., 57, (2018) 21.
[29] W. J. Tsai, C. J. Gu, C. W. Cheng, and J. B Horng: Opt. Eng., 53, (2014) 5.
[30] J. Dudutis, R. Stonys, G. Račiukaitis, and P. Gečys: Procedia CIRP, 74 (2018).
[31] J. Dudutis, P. Gečys, and G. Račiukaitis: Opt. Express, 24, (2016).
[32] K. Poder, J. M. Cole, J. C., S. Alatabi, P. S. Foster, C., Kamperidis, O. Kononenko, C. A. Palmer, D. Rusby, A. Sahai, G. Sarri, D. R. Symes, J. R., Warwick, S. P. D. Mangles, and Z. Najmudin: Plasma Phys. Control. Fusion, 60, (2017) 1.
[33] Y. Yang, D. Franz, C. Esen, and R. Hellmann: J. Laser Appl., 35, (2023) 4.
[34] Y. Yang, D. Franz, C. Esen, and R. Hellmann: J. Intell. Manuf., 36, (2025) 4.
[35] M. Shimizu, M. Sakakura, M. Ohnishi, Y. Shimotsuma, T. Nakaya, K. Miura, and K. Hirao: J. Appl. Phys., 108, (2010) 7.
[36] M. Sakakura, Y. Shimotsuma, and K. Miura: J. Laser Micro Nanoeng., 12, (2017) 2.
[37] N. M. Bulgakova, V. P. Zhukov, A. R. Collins, D. Rostohar, T. J. Y. Darrien, and T. Mocek: Appl. Surf. Sci., 336, (2015).
[38] D. Moskal, J. Martan, M. Honner, C. Beltrami, M. J. Kleefoot, and V. Lang. M. Int. J. Heat Mass Transf., 213, (2023) 124328.
[39] M. Sun, U. Eppelt, C. Hartmann, W. Schulz, J. Zhu, and Z.Lin: Opt. Laser Technol., 80, (2016).

[40] Y. Ito, R. Shinomoto, K. Nagato, A. Otsu, K. Tatsukoshi, Y. Fukasawa, T. Kizaki, N. Sugita, and M. Mitsuishi: Appl. Phys. A, 124, (2018).
[41] R. Weber, T. Graf, P. Berger, V. Onuseit, M. Wiedenmann, C. Freitag, and A. Feuer: Opt. Express, 22, (2014) 9.
[42] Y. Yang, D. Franz, C. Esen and R. Hellmann: J. Laser Micro Nanoeng., 20, (2025) 2.
[43] D. Franz, Y. Yang, L. Michel, C. Esen, and R. Hellmann: J. Laser Appl., 35, (2023) 4.